https://doi.org/10.5194/egusphere-2026-3299
Preprint. Discussion started: 6 August 2026

Decadal transition of $PM_{2.5}$ source structure over North China: Weakening combustion and emerging nitrate-driven pollution

Yuchen Li[1,9], Zheng Zong[2], Xiaoping Wang[3], Xiaolan Shi[4,5], Zeyu Sun[6,7], Zhineng Cheng[8], Ziyang Zhang[8,9], Xuehua Yin[1,9], Zhifeng Lou[1,9], Rong Sun[1], Roland Kallenborn[10], and Chongguo Tian[1]

[1]Shandong Key Laboratory of Coastal Environmental Processes, CAS Key Laboratory of Coastal Environmental Processes and Ecological Remediation, Yantai Institute of Coastal Zone Research, Chinese Academy of Sciences, Yantai 264003, China
[2]Environmental Research Institute, Shandong University, Qingdao 266237, Shandong, China
[3]School of Resource and Environmental Engineering, Ludong University, Yantai 264025, China
[4]Frontiers Science Center for Deep Ocean Multispheres and Earth System, and Key Laboratory of Marine Chemistry Theory and Technology, Ministry of Education (MOE), Ocean University of China, Qingdao 266100, China
[5]Laboratory of Marine Ecology and Environmental Science, Qingdao National Laboratory for Marine Science and Technology, Qingdao 266237, China
[6]Zhejiang Environment Technology Co., Ltd., Hangzhou 311100, China
[7]College of Environmental & Resource Sciences, Zhejiang University, Hangzhou, Zhejiang 310058, China
[8]State Key Laboratory of Advanced Environmental Technology, Guangzhou Institute of Geochemistry, Chinese Academy of Sciences, Guangzhou 510640, China
[9]University of Chinese Academy of Sciences, Beijing 100049, China
[10]Norwegian University of Life Sciences, Faculty of Chemistry, Biotechnology and Food Sciences, Christian Magnus Falsens vei 18, 1433 Ås, Norway

Correspondence to: Chongguo Tian (cgtian@yic.ac.cn)

Abstract. Long-term clean-air actions have reshaped fine-particle pollution in North China, but it remains unclear how the source structure of $PM_{2.5}$ has changed at the regional background scale and which chemical components are amplified. We combine long-term observations from Tuoji Island (2012–2023), a coastal background site, with chemical analysis, positive matrix factorization (PMF), ion balance, and thermodynamic diagnostics. Although $PM_{2.5}$ mass did not decrease monotonically, its composition and source structure changed substantially. Elemental carbon decreased from 1.46 to 0.81 μg m^{-3}, and the biomass/coal combustion contribution decreased from 43.37 % to 13.74 %, indicating weakened primary-combustion signals. SO_4^{2-} decreased from 9.86 to 4.10 μg m^{-3}, while the NO_3^-/SO_4^{2-} ratio increased from 0.64 to 2.08, showing a shift from sulfate dominance toward greater nitrate importance. After mineral-dust outliers were removed, NO_3^- accounted for 19.19 % of $PM_{2.5}$ in the highest 20 % of samples during 2021–2023, and the PMF secondary nitrate contribution reached 27.59 %, making it the dominant amplified source factor. Greater NH_4^+ excess and model-diagnosed aerosol liquid water content indicate increased NH_4^+ availability after sulfate neutralisation and wetter particles, favouring NH_4NO_3 formation and persistence. These findings show that emission reductions reorganised $PM_{2.5}$ pollution toward weaker primary combustion and sulfate influence but stronger nitrate amplification during late-stage high-$PM_{2.5}$ conditions.

Keywords. Tuoji Island; $PM_{2.5}$; positive matrix factorization; source-structure reorganisation; secondary nitrate; ion balance

1 Introduction

Fine particulate matter ($PM_{2.5}$) remains a major obstacle to further air-quality improvement in China because of its adverse effects on visibility and human health (Pui et al., 2014). Over the past decade, China has implemented the Air Pollution Prevention and Control Action Plan and the Three-Year Action Plan for Winning the Blue Sky Defence Battle, with sustained controls on coal combustion, industrial emissions, vehicle emissions, and residential solid-fuel use. According to national

https://doi.org/10.5194/egusphere-2026-3299
Preprint. Discussion started: 6 August 2026

emission inventories, emissions of SO_2, NO_x, CO, and primary particulate matter have declined during these clean-air action periods, with particularly strong reductions in SO_2 (Kong et al., 2024). However, heavy-pollution episodes have not disappeared; instead, their dominant components and control challenges have changed (Meng et al., 2022; Zhai et al., 2021). The updated Technical Regulation on Ambient Air Quality Index (AQI), implemented on 1 March 2026, further tightened $PM_{2.5}$ AQI breakpoints (MEE, 2026), increasing the need to identify the factors that constrain $PM_{2.5}$ reduction.

North China is one of the key regions for $PM_{2.5}$ control. The policy focus has gradually shifted from primary-emission reduction toward coordinated precursor control and mitigation of secondary aerosol formation. Long-term observations indicate that primary combustion and sulfate-related contributions have weakened in North China, including representative cities such as Tianjin and Beijing, while nitrate has become increasingly important. In Tianjin, for example, the sulfate fraction in $PM_{2.5}$ decreased from 15.0 % to 9.6 % during 2013–2019, whereas the nitrate fraction increased from 12.5 % to 15.8 %, accompanied by an increase in the NO_3^-/SO_4^{2-} ratio (Dai et al., 2023). A decade-long record in Beijing showed a similar pattern: although NO_3^-, SO_4^{2-}, and NH_4^+ generally decreased during 2011–2020, the decline rate of SO_4^{2-} was 8.80 % yr^{-1}, larger than that of NO_3^- at 5.10 % yr^{-1}. The NO_3^-/SO_4^{2-} ratio exceeded 1 under many pollution levels and increased over time (Wang et al., 2022). Nitrate formation has therefore become central to explaining persistent $PM_{2.5}$ pollution in China. Recent studies show that nitrate in North China is influenced by trans-regional NO_2 transport, springtime soil NO_x pulses, industrial-stack NH_3 emissions under strong oxidation, and gas-phase OH and heterogeneous N_2O_5 pathways (Xiao et al., 2025; Feng et al., 2025; Yang et al., 2025; Cao et al., 2025). These findings indicate that late-stage nitrate pollution is controlled by coupled precursor emissions, oxidation chemistry, ammonia availability, regional transport, and gas-particle partitioning rather than by a single local source or process.

Nevertheless, most existing source-apportionment studies focus on single years, seasons, or typical pollution events at urban sites, which are strongly influenced by local emissions. Long-term (>10 years) records of source structure evolution at regional background sites – where the integrated signal of continental outflow after transport and atmospheric processing can be captured – remain rare. In particular, it is still unclear how the source structure of $PM_{2.5}$ has changed at the regional background scale over the full period of China's clean-air actions, and which chemical components or source factors are preferentially amplified during high-$PM_{2.5}$ episodes in the later stage of emission controls. Although declines in combustion-related sources and sulfate alongside rising nitrate have been widely reported (Zhai et al., 2021; Meng et al., 2022; Liu et al., 2025), whether this transition is persistent at the regional background scale, and how it relates to primary-emission control, secondary-inorganic-aerosol adjustment, regional transport, and coastal processing across the key stages following the 2013 clean-air action and the post-2018 deepening of controls, remains insufficiently constrained by long-term evidence.

Long-term observations at regional background sites are therefore needed to separate persistent compositional changes from short-term meteorological variability. Compared with urban sites, coastal and island background stations are less directly affected by intense local emissions and better record the integrated signal of continental outflow after transport, mixing, and atmospheric processing, and are well suited to identifying regional transport, sea-salt displacement, and coastal secondary formation (Chang et al., 2018; Liu et al., 2020; Yen et al., 2024). Previous coastal and island studies have shown that sea-salt particles undergo ion displacement during transport, that chloride can be replaced by nitrate, and that shipping, continental outflow, and secondary formation may overlap at coastal sites (Li et al., 2018; Zhang et al., 2021; Wu et al., 2024). Tuoji Island, in the central Bohai Strait, lies where North China continental outflow, cross-regional transport from the Beijing–Tianjin–Hebei region and Shandong Peninsula, and coastal atmospheric processes converge, making it well suited to record the regional response of transported continental pollutants together with sea-salt input, land–sea mixing, and particle-phase processing.

To address these gaps, this study uses a unified chemical-composition dataset from Tuoji Island, a coastal background site in the central Bohai Strait, covering the period 2012–2023. We aim to answer three specific scientific questions: (1) has the $PM_{2.5}$ source structure undergone a qualitative change over time, even though the mass concentration did not decrease monotonically?

https://doi.org/10.5194/egusphere-2026-3299
Preprint. Discussion started: 6 August 2026

(2) during high-$PM_{2.5}$ episodes (after excluding mineral-dust outliers), which chemical component or PMF-resolved source factor is selectively amplified, and how does this amplification change from the early to the late stage? (3) have the chemical and thermodynamic conditions favouring nitrate formation – such as ammonium availability, aerosol liquid water content, and the degree of sulfate neutralisation – systematically shifted from the early to the late stage?

By combining long-term chemical observations, PMF source apportionment, ion-balance and ISORROPIA-II diagnostics, and a stage-level comparison of high-$PM_{2.5}$ samples, we provide background-scale evidence on the reorganisation of $PM_{2.5}$ source structure under emission reductions. The results are expected to inform coordinated control strategies for $PM_{2.5}$ under the new air-quality framework, particularly regarding the growing role of secondary nitrate.

2 Materials and methods

2.1 Study area and sample collection

$PM_{2.5}$ samples were collected on Tuoji Island from March 2012 to August 2013 and from September 2017 to February 2024. The site is located in the central Bohai Strait (37.98° N, 120.73° E; Fig. S1), about 40 km from Penglai and 70 km from Dalian. Important shipping channels, including Laotieshan Channel, Changshan Channel, and Miaodao Strait, are located nearby, and several large ports, including Dalian, Yingkou, Tianjin, Qinhuangdao, and Qingdao, are distributed around the Bohai Sea. The sampler was installed on the highest hill of the island, about 153 m above sea level and about 3 km from local residential areas. The site is less directly influenced by local anthropogenic emissions and is suitable for recording the composition of $PM_{2.5}$ after regional transport, mixing, and coastal processing.

Samples were collected with a high-volume sampler (Hi-Vol 3000, Ecotech Company, Australia) on quartz-fibre filters (Whatman QM-A, 8 × 10 in.). Prior to sampling, filters were pre-baked at 500 °C for 4 h to remove background organic contamination. The sampling flow rate was 1.13 m^3 min^{-1}, and each sample was collected for 24 h, nominally every 3 d. Because of instrument maintenance, changes in sampling conditions during the COVID-19 period, and the exclusion of invalid or incomplete samples, the sequence is not fully continuous. After checks of sample validity and component completeness, 672 valid samples were used for stage-level statistics.

All filters were equilibrated in a temperature- and humidity-controlled chamber at 25 ± 1 °C and 50 ± 2 % relative humidity for 24 h before and after sampling and were weighed using a Sartorius MC5 electronic microbalance. Each filter was weighed at least three times. The repeated weighing difference was controlled within 20 μg for sampled filters and 10 μg for blank filters (Zong et al., 2016). After weighing, the filters were folded, wrapped in aluminium foil, sealed in plastic bags, and stored at −20 °C until chemical analysis.

2.2 Chemical analysis and quality control

Organic carbon (OC) and elemental carbon (EC) were measured using a thermal–optical carbon analyser following the IMPROVE_A protocol (Chow et al., 2007). Major water-soluble inorganic ions were measured by ion chromatography (Wang et al., 2006). For trace-element analysis, a separate 61.8 cm^2 filter section was digested with 10 mL of high-purity HNO_3 at 120 °C for 120 min; after cooling, the digest was filtered, diluted to 50 mL, and analysed by inductively coupled plasma mass spectrometry (ICP-MS) (Zong et al., 2016; Wang et al., 2006). The measured species included SO_4^{2-}, NO_3^-, NH_4^+, Na^+, Cl^-, Mg^{2+}, Ca^{2+}, K^+, V, Cr, Mn, Fe, Ni, Cu, Zn, As, Cd, and Pb. Field blanks, laboratory blanks, replicate samples, and internal standards were used for quality control, and concentrations were blank-corrected before statistical analysis and PMF modelling. Al, Si, Ti, and some refractory components were not measured, and OC represents carbon rather than total organic matter. Detailed analytical procedures, detection limits, analytical uncertainties, and blank values are provided in Text S1.

https://doi.org/10.5194/egusphere-2026-3299
Preprint. Discussion started: 6 August 2026

2.3 Meteorological data and stage definition

Ground meteorological data were obtained from the Tuoji Island monitoring station using an FRT FWS-series automatic weather station. The system measured air temperature, relative humidity, air pressure, and wind speed and direction; the resolutions of temperature, relative humidity, and wind speed were 0.1 °C, 0.1 % RH, and 0.1 m s^{-1}, respectively. Quality-controlled station records were aggregated to daily values and matched to $PM_{2.5}$ sampling dates. Relative humidity and temperature were used in ISORROPIA-II diagnostics, and wind speed supported interpretation of coastal dispersion and transport.

The three analysis periods were defined according to sample continuity, temporal coverage, and the timeline of regional air-pollution control. The 2012–2013 period predates the full implementation of the Air Pollution Prevention and Control Action Plan and represents the pre-action background state. Samples from 2014–2016 were insufficient in number and temporal coverage for a separate stage analysis and were therefore not used for stage-mean comparison. The 2017–2020 period provides a relatively complete sequence during the further strengthening of clean-air controls. The 2021–2023 period follows the completion of the Three-Year Action Plan and is used to examine later-stage changes in source contributions and high-$PM_{2.5}$ samples. The three stages include 119, 263, and 290 valid samples, respectively. To identify components and sources amplified during high-$PM_{2.5}$ conditions, the highest 20 % of $PM_{2.5}$ samples within each stage were defined as high-$PM_{2.5}$ samples after mineral-dust outlier screening, as described in Sect. 2.6.

2.4 Ion balance and thermodynamic diagnostics

To evaluate how sulfate weakening may have altered particulate NH_4^+ availability, we calculated the molar $n(NH_4^+)/2n(SO_4^{2-})$ ratio and NH_4^+ excess using sample-level SO_4^{2-}, NO_3^-, and NH_4^+ data, following previous ion-neutralisation and excess-ammonium diagnostics (Pathak et al., 2009; Wu et al., 2015). Mass concentrations were converted using $n(NH_4^+) = [NH_4^+]/18$ and $n(SO_4^{2-}) = [SO_4^{2-}]/96$. The ratio indicates whether particulate NH_4^+ is sufficient to neutralise SO_4^{2-} as $(NH_4)_2SO_4$, while NH_4^+ excess, calculated as $n(NH_4^+) - 2n(SO_4^{2-})$, quantifies NH_4^+ remaining after sulfate neutralisation. Positive values indicate conditions favourable for NH_4NO_3 formation; negative values indicate sulfate-constrained NH_4^+. These particle-phase stoichiometric indicators do not represent gas-phase NH_3 or independently demonstrate gas–particle partitioning.

ISORROPIA-II was used to diagnose aerosol liquid water content (ALWC) and aerosol acidity (pH) (Fountoukis and Nenes, 2007) from particle-phase Na^+, SO_4^{2-}, NH_4^+, NO_3^-, Cl^-, Ca^{2+}, K^+, and Mg^{2+} and date-matched relative humidity and temperature. Reverse-mode calculations used the observed particle-phase composition and meteorology to constrain the inorganic aerosol thermodynamic state. Metastable results were used for ALWC, and stable results for model-resolved solid salts. Detailed thermodynamic inputs and outputs are provided in Text S4, Table S6, and Fig. S7.

2.5 PMF input matrix and source apportionment

$PM_{2.5}$ source apportionment was performed using EPA PMF 5.0 (Paatero and Tapper, 1994; Paatero, 1997; Norris et al., 2014). PMF decomposes the observed concentration matrix at the receptor site into a source-profile matrix and a source-contribution matrix by minimising an objective function. The model is expressed as Eq. (1):

$$x_{ij} = \sum_{k=1}^{p} g_{ik} f_{kj} + e_{ij} \qquad (1)$$

where x_{ij} is the observed concentration of species j in sample i, g_{ik} is the contribution of source k to sample i, f_{kj} is the profile of species j in source k, e_{ij} is the residual, and p is the number of factors.

Values below the method detection limit (MDL) were not deleted. For the PMF input matrix, concentrations lower than or equal to the MDL were replaced by half of the MDL. Uncertainties were calculated using Eq. (2) for concentrations lower than or equal to the MDL and Eq. (3) for concentrations higher than the MDL (Norris et al., 2014). For descriptive statistics, blank-

https://doi.org/10.5194/egusphere-2026-3299
Preprint. Discussion started: 6 August 2026

corrected valid concentrations were used. This treatment avoids setting low values to zero and accounts for the larger uncertainty of low-concentration measurements in PMF.

$$Unc = \frac{5}{6} \times MDL \qquad (2)$$

$$Unc = \sqrt{(ErrorFraction \times concentration)^2 + (0.5 \times MDL)^2} \qquad (3)$$

where Unc is the species-specific uncertainty, MDL is the method detection limit, ErrorFraction is the analytical error fraction, and concentration is the blank-corrected concentration.

The PMF variables included $PM_{2.5}$ mass, OC, EC, eight major water-soluble inorganic ions, and ten trace elements. $PM_{2.5}$ and the trace elements were treated as weak variables, whereas OC, EC, and the water-soluble ions were treated as strong variables. The combined measurements of major ions, OC/EC, and acid-digested trace elements provide complementary tracers for secondary aerosol, combustion, mineral dust, sea salt, port-related emissions, and industrial-metal sources, thereby supporting the source apportionment conducted here, as in previous PMF applications at regional background and coastal sites (Zong et al., 2016; Liu et al., 2022). Only samples for which all common PMF input species and corresponding uncertainty estimates were available were retained in the PMF input matrix, resulting in 313 samples (Table S2). Because this requirement made the PMF sample set smaller than the full valid sample set used in Sect. 3.1, source-contribution comparisons were made for comparable PMF periods: 2012, 2019–2020, and 2021–2023, rather than for the full 2017–2020 composition stage. These comparisons were used to examine whether the compositional changes observed in the full data set were also reflected in source contributions within the comparable PMF subset.

Factor-number tests covered 4–8 factors. The unrotated seven-factor Base solution was adopted as the main PMF solution: the six-factor solution merged sea-salt-, port-, and metal-related signals, whereas the eight-factor solution over-separated sea-salt-, metal-, and nitrate-related signals. Fpeak = 0.5 was retained only as a rotational sensitivity test. Across stage-average and dust-screened high-$PM_{2.5}$ samples, the maximum absolute difference in relative factor contributions between the Base and Fpeak = 0.5 solutions was 0.59 percentage points. Bootstrap mapping rates were 85 %–100 %, and DISP returned error code 0 with no factor swaps; all Fpeak profile values lay within the corresponding dQ = 4 DISP intervals of the Base solution (Norris et al., 2014; Brown et al., 2015). Full diagnostics are provided in Text S2, Tables S2 and S3a–S3c, and Figs. S2a–S3.

The final factor names and chemical-profile interpretations are given in Sect. 3.2. Factor naming was based on chemical-profile characteristics, site context, and previous studies at coastal, port, and regional background sites.

2.6 Statistical analysis

Descriptive statistics summarised annual and stage-level changes in $PM_{2.5}$ mass, chemical components, and PMF source contributions. Changes in secondary inorganic aerosol were assessed using the NO_3^-/SO_4^{2-} ratio and the combined SO_4^{2-}, NO_3^-, and NH_4^+ fraction of $PM_{2.5}$. Stage differences were tested using the Kruskal–Wallis H test followed by pairwise Mann–Whitney U tests; all p values were two-sided. Bootstrap resampling was used to estimate 95 % confidence intervals for stage-mean differences and to assess the robustness of stage-level changes.

To avoid the influence of dust-event samples on the definition of high-$PM_{2.5}$ samples, mineral-dust outliers were screened before high-$PM_{2.5}$ selection. DeBell et al. (2004) reported that, during Asian dust transport events, bulk aerosol water-soluble Ca^{2+} exceeded the site-specific multiyear 95th percentile on every event day at AIRMAP stations. At IMPROVE sites, $PM_{2.5}$ elemental Ca and Fe exceeded at least the 90th percentile and were frequently above the 95th percentile. Following this high-percentile mineral-dust outlier-screening logic, and to reduce the possibility of misclassification based on a single tracer, this study calculated the 95th percentiles of water-soluble Ca^{2+} and elemental Fe for the full sample sequence. Samples in which both water-soluble Ca^{2+} and elemental Fe exceeded their respective 95th-percentile thresholds were labelled as mineral-dust outliers. These samples were removed within each stage, and the highest 20 % of remaining $PM_{2.5}$ samples were then defined

https://doi.org/10.5194/egusphere-2026-3299
Preprint. Discussion started: 6 August 2026

as high-$PM_{2.5}$ samples. The removed dates, threshold sensitivity, and seasonal checks are given in Text S3, Tables S4a–S5, and Figs. S4–S5.

3 Results and discussion

3.1 Stage-dependent changes in $PM_{2.5}$ and major chemical components

Following the stage definition in Sect. 2.3, we compare stage-level changes in $PM_{2.5}$ mass, carbonaceous components, water-soluble inorganic ions, and high-$PM_{2.5}$ sample composition across 2012–2013, 2017–2020, and 2021–2023. Stage-level changes in key components are shown in Fig. 1 and Table S1.

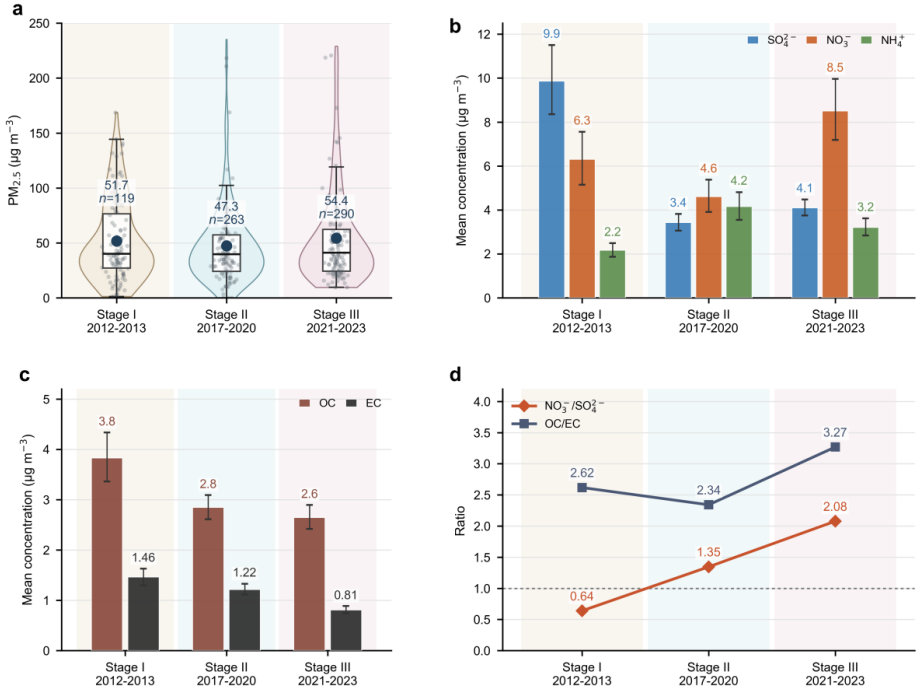

Figure 1. Stage-level changes in $PM_{2.5}$ and key chemical components at Tuoji Island during 2012–2023. (a) $PM_{2.5}$ distributions and stage means; (b) stage-mean concentrations of major water-soluble ions SO_4^{2-}, NO_3^-, and NH_4^+; (c) stage-mean concentrations of carbonaceous components OC and EC; (d) NO_3^-/SO_4^{2-} and OC/EC ratios. Shading indicates the three stages used in this study, and n denotes the number of valid samples in each stage.

Changes in carbonaceous components provide evidence for a weakening of primary-combustion signals. The stage-mean OC concentration decreased from 3.83 ± 2.73 μg m^{-3} in 2012–2013 to 2.85 ± 1.95 μg m^{-3} in 2017–2020 and further to 2.65 ± 2.05 μg m^{-3} in 2021–2023. Elemental carbon (EC) decreased from 1.46 ± 0.94 μg m^{-3} to 1.22 ± 0.90 and 0.81 ± 0.62 μg m^{-3}. Compared with OC, EC showed a more consistent decline across the three stages, and stage differences were statistically significant ($p < 0.001$, Kruskal–Wallis test). Because EC is commonly used as an indicator of primary combustion emissions, the long-term decline points to weakened combustion-related carbonaceous signals at Tuoji Island (Cao et al., 2005; Liu et al., 2022).

Among water-soluble ions, sulfate and nitrate showed the clearest relative changes. In 2012–2013, stage-mean SO_4^{2-} and NO_3^- concentrations were 9.86 ± 8.33 and 6.31 ± 6.42 μg m^{-3}, respectively, with a NO_3^-/SO_4^{2-} ratio of 0.64. In 2017–2020, SO_4^{2-} decreased to 3.42 ± 3.14 μg m^{-3}, while NO_3^- was 4.61 ± 6.05 μg m^{-3} and the NO_3^-/SO_4^{2-} ratio increased to 1.35. By 2021–2023, SO_4^{2-} was 4.10 ± 3.13 μg m^{-3}, NO_3^- increased to 8.51 ± 11.60 μg m^{-3}, and the NO_3^-/SO_4^{2-} ratio further increased to

https://doi.org/10.5194/egusphere-2026-3299
Preprint. Discussion started: 6 August 2026

2.08. SO_4^{2-} was significantly lower than in the early stage ($p < 0.001$), whereas NO_3^- and its fraction in $PM_{2.5}$ were significantly higher in 2021–2023 than in 2017–2020 ($p < 0.001$). The late-stage change was therefore not a rebound of primary-combustion components, but a higher relative importance of nitrate after sulfate dominance weakened. Similar nitrate enhancement has been reported in recent long-term observations in North China (Dai et al., 2023; Meng et al., 2022; Zhai et al., 2021).

The stage-dependent behaviour of NH_4^+ differed from that of both sulfate and nitrate. Its stage means were 2.16 ± 1.64, 4.16 ± 5.24, and 3.21 ± 3.30 μg m^{-3}, showing neither a synchronous decrease with SO_4^{2-} nor a synchronous increase with NO_3^-. Because NH_4^+ participates in both ammonium sulfate and ammonium nitrate formation, its variation can be affected by sulfate reduction, nitrate accumulation, NH_3 supply, and gas–particle partitioning. The fact that NH_4^+ remained higher than in the early stage despite the SO_4^{2-} decrease suggests that sulfate constraints on ammonium may have weakened, but this requires further ion-balance and thermodynamic diagnostics.

High-$PM_{2.5}$ episodes are associated with reduced visibility and increased health risk. Identifying the components amplified during these episodes helps clarify pollution formation and subsequent control priorities. Before defining high-$PM_{2.5}$ samples, mineral-dust outliers were removed using the concurrent-anomaly criterion based on water-soluble Ca^{2+} and elemental Fe, as described in Sect. 2.6. After removing these samples, the highest 20 % of $PM_{2.5}$ samples within each stage were selected as high-$PM_{2.5}$ samples (Fig. 2a). This procedure identified and removed 2, 0, and 6 mineral-dust outliers in 2012–2013, 2017–2020, and 2021–2023, respectively; the removed dates are provided in Text S3. After removal, 117, 263, and 284 samples remained for high-$PM_{2.5}$ selection, giving 24, 53, and 57 high-$PM_{2.5}$ samples, respectively. Comparison with official dust-event bulletins from the China Meteorological Administration and public weather records showed that most samples with concurrent anomalies in water-soluble Ca^{2+} and elemental Fe coincided with, or occurred close to, regional dust, blowing-sand, or floating-dust episodes, supporting the validity of the screening rule.

To examine the robustness of the 20 % threshold, sample size, seasonal-stratification stability, and major component fractions were compared under the highest 10 %, 20 %, and 30 % $PM_{2.5}$ thresholds after removing mineral-dust outliers. Details are provided in Text S3, Tables S4a and S4b, and Fig. S4. Wilson and Agresti–Coull proportion intervals and Cochran's rule for minimum expected cell frequencies show that the highest 10 % threshold produced too few samples for stable seasonal stratification. In 2012–2013, for example, the highest 10 % contained only 12 samples, so one sample represented 8.3 % of the subset; after seasonal grouping, spring, winter, summer, and autumn contained 5, 3, 3, and 1 samples, respectively. The 10 % threshold better captures extreme high-$PM_{2.5}$ events but is unsuitable as the main threshold for stage comparison and seasonal sensitivity analysis. A fixed concentration threshold of 75 μg m^{-3}, corresponding to the 24 h Grade II $PM_{2.5}$ limit specified in GB 3095–2012 (MEP, 2012), was also used for comparison. In 2021–2023, 55 samples exceeded 75 μg m^{-3}, close to the 57 samples selected by the highest 20 % threshold. Their NO_3^- fraction, SO_4^{2-} fraction, and NO_3^-/SO_4^{2-} ratio were also broadly consistent with the 20 % result. By contrast, the highest 30 % threshold included more medium-concentration samples; in 2021–2023, 31 samples in the highest 30 % group were below 75 μg m^{-3}. Considering sample number, seasonal-stratification stability, high-$PM_{2.5}$ identification, and fixed-threshold comparison, the highest 20 % was used for subsequent high-$PM_{2.5}$ composition and source analyses.

High-$PM_{2.5}$ samples were mainly concentrated in winter and spring. This seasonal distribution is consistent with pollution formation conditions in North China: winter heating, combustion emissions, and high NO_x levels increase precursor supply, while low temperature, high humidity, shallow boundary layers, and poor dispersion favour NH_4NO_3 partitioning to the particle phase and pollutant accumulation (Gao et al., 2016; Tang et al., 2021). Spring high-$PM_{2.5}$ episodes may also be affected by regional transport and mineral dust. Coastal megacity observations in North China show that spring pollution often reflects mixing between anthropogenic pollutants and dust or regionally transported aerosols (Su et al., 2017). Seasonal sensitivity analysis showed that the NO_3^-/SO_4^{2-} ratio increased in both spring and winter high-$PM_{2.5}$ samples in the later stage (Fig. S5), indicating that nitrate enhancement relative to sulfate was not simply caused by differences in seasonal distribution.

https://doi.org/10.5194/egusphere-2026-3299
Preprint. Discussion started: 6 August 2026

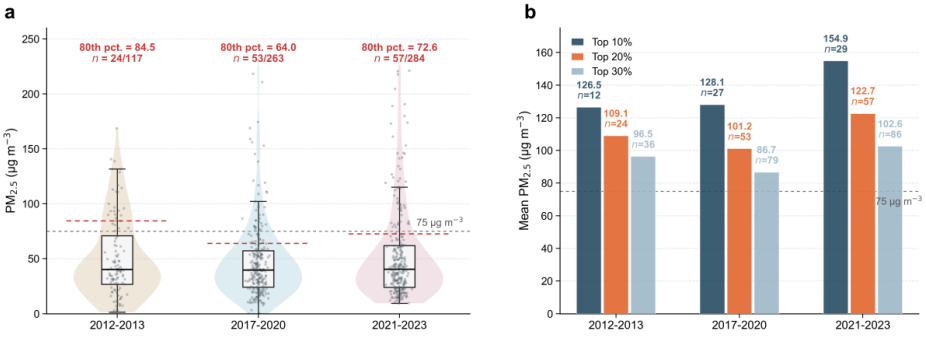

Figure 2. Identification and sensitivity tests for high-$PM_{2.5}$ samples after removal of mineral-dust outliers. (a) $PM_{2.5}$ distributions, 80th-percentile thresholds, and numbers of high-$PM_{2.5}$ samples in each stage; (b) mean $PM_{2.5}$ concentrations and sample numbers under the highest 10 %, 20 %, and 30 % thresholds. The dashed line indicates the fixed concentration reference of 75 μg m^{-3}.

The contrast among components became clearer in high-$PM_{2.5}$ samples. In 2012–2013, SO_4^{2-}, NO_3^-, and OC+EC accounted for 17.63 %, 13.41 %, and 9.52 % of $PM_{2.5}$ in high-$PM_{2.5}$ samples, respectively, so both sulfate and nitrate were important in early high-$PM_{2.5}$ samples and nitrate had not yet become dominant. In 2017–2020, the NO_3^- fraction was 10.48 %, already higher than the SO_4^{2-} fraction of 5.81 %, and the NH_4^+ fraction reached 9.71 %. By 2021–2023, NO_3^- accounted for 19.19 % of $PM_{2.5}$, clearly higher than SO_4^{2-} at 5.97 % and OC+EC at 5.29 % (Fig. 3a). Because component enhancement during high-$PM_{2.5}$ events can be expressed in terms of both concentration and relative abundance, the enrichment factor here was defined as the ratio of the component mass fraction in high-$PM_{2.5}$ samples to that in screened stage-average samples. Compared with screened stage-average conditions, the NO_3^- enrichment factor reached 1.54 in 2021–2023, whereas SO_4^{2-} and OC+EC had enrichment factors of only 0.62 and 0.73 (Fig. 3b). The NO_3^-/SO_4^{2-} ratios in high-$PM_{2.5}$ samples were 0.76, 1.77, and 3.42 in 2012–2013, 2017–2020, and 2021–2023, respectively, all higher than the corresponding screened stage-average values of 0.63, 1.35, and 2.05 (Fig. 3c). Taken together, these results show that nitrate was the key $PM_{2.5}$ component in the late stage and the most strongly amplified component in late-stage high-$PM_{2.5}$ samples.

In addition to carbonaceous components and major water-soluble ions, Na^+, Cl^-, Mg^{2+}, Ca^{2+}, Fe, and trace metals provide evidence for identifying sea-salt, mineral-dust, port-emission, and industrial-metal factors in the PMF analysis. These tracer species help characterise the coastal setting and regional inputs at Tuoji Island, but the stage-to-stage shift in $PM_{2.5}$ composition is more directly reflected in the increasing NO_3^-/SO_4^{2-} ratio and the selective nitrate amplification in high-$PM_{2.5}$ samples. Overall, Sect. 3.1 shows that $PM_{2.5}$ composition at Tuoji Island changed markedly during 2012–2023: primary-combustion carbon signals weakened, sulfate dominance declined, and nitrate became more prominent, especially in late-stage high-$PM_{2.5}$ samples. Sect. 3.2 further examines whether these chemical changes are reflected in PMF-resolved source contributions and in the source structure of high-$PM_{2.5}$ samples.

https://doi.org/10.5194/egusphere-2026-3299
Preprint. Discussion started: 6 August 2026

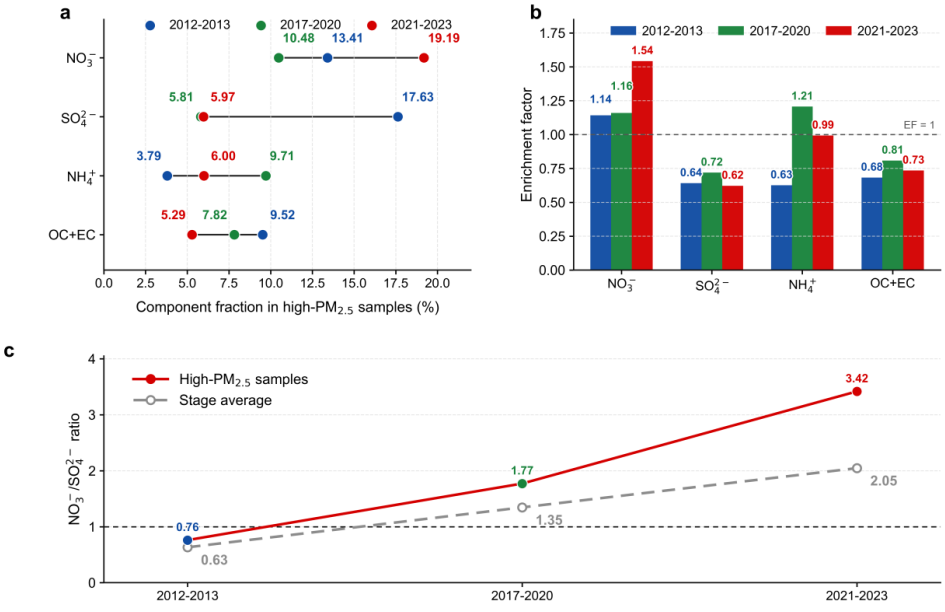

Figure 3. Composition, enrichment, and NO_3^-/SO_4^{2-} changes in high-$PM_{2.5}$ samples after mineral-dust outlier removal. (a) Fractions of NO_3^-, SO_4^{2-}, NH_4^+, and OC+EC in high-$PM_{2.5}$ samples; (b) enrichment factors of major components in high-$PM_{2.5}$ samples relative to the screened stage-average level; (c) NO_3^-/SO_4^{2-} ratios in high-$PM_{2.5}$ samples and screened stage-average samples.

3.2 Evolution of $PM_{2.5}$ source structure at the coastal background site

The unrotated seven-factor Base solution selected in Sect. 2.5 was used as the main PMF solution. The resolved factors were F1 secondary sulfate, F2 biomass/coal combustion, F3 mineral dust, F4 secondary nitrate, F5 sea salt, F6 port emissions, and F7 industrial metals. Detailed factor-profile interpretation and the chemical profiles are provided in Text S2 and Fig. S3. Briefly, secondary sulfate and secondary nitrate were identified by sulfate- and nitrate-rich profiles with associated ammonium. Biomass/coal combustion was characterised by K^+, OC, EC, and coal-combustion-related tracers; mineral dust by Ca^{2+}, Fe, and Mg^{2+}; sea salt by Na^+, Cl^-, and Mg^{2+}; port emissions by Na^+, Fe, Ni, and Cu; and industrial metals by Cr, Mg^{2+}, Fe, Ni, Cu, Zn, As, and Cd.

Stage-average PMF contributions show that early $PM_{2.5}$ mass was mainly influenced by biomass/coal combustion and secondary sulfate. In 2012, the relative contributions of biomass/coal combustion, secondary sulfate, port emissions, and secondary nitrate were 43.37 %, 28.76 %, 12.02 %, and 5.50 %, respectively. In 2019–2020, biomass/coal combustion decreased to 15.03 %, secondary sulfate was 24.90 %, secondary nitrate increased to 17.18 %, and port emissions increased to 26.40 %. In 2021–2023, port emissions remained relatively high at 27.15 %, secondary sulfate was 22.99 %, secondary nitrate was 16.59 %, and biomass/coal combustion further decreased to 13.74 %. The clearest stage-average change is the sustained weakening of the biomass/coal combustion factor. At the same time, secondary nitrate changed from a low-contribution factor in the early stage to an important $PM_{2.5}$ source in the middle and late stages. The relative contribution of secondary sulfate did not decrease as strongly as its mass concentration. This difference may reflect the combined variation of sulfate, ammonium, and regional transport processes within the PMF factor, so it should not be interpreted as a simple decline of a single source.

The port-emission, sea-salt, and industrial-metal factors should be distinguished from the source-structure reorganisation central to this study. The sea-salt factor mainly reflects the coastal background, the port-emission factor captures the combined influence of port and shipping activities, ship-fuel combustion, coastal aerosol, and regional metal inputs, and the industrial-metal factor mainly records trace-metal signals. These factors help explain the site characteristics and regional inputs at Tuoji

https://doi.org/10.5194/egusphere-2026-3299
Preprint. Discussion started: 6 August 2026

Island, but cannot alone explain the increasing NO_3^-/SO_4^{2-} ratio or the marked increase in the nitrate fraction of late-stage high-$PM_{2.5}$ samples.

The high-$PM_{2.5}$ PMF results, based on 11, 17, and 35 dust-screened samples from the PMF input subset in 2012, 2019–2020, and 2021–2023, respectively, are consistent with the component-based evidence in Sect. 3.1 (Fig. 4). In 2012, the relative contributions of biomass/coal combustion, secondary sulfate, and secondary nitrate were 47.39 %, 27.50 %, and 7.57 %, indicating that early high-$PM_{2.5}$ conditions were still mainly influenced by combustion emissions and sulfate-related processes. In 2019–2020 high-$PM_{2.5}$ samples, secondary nitrate increased to 21.50 %, becoming comparable to secondary sulfate (20.38 %), biomass/coal combustion (19.91 %), and port emissions (19.89 %). By 2021–2023, secondary nitrate increased to 27.59 %, higher than biomass/coal combustion (18.36 %), port emissions (18.02 %), and secondary sulfate (16.59 %); its enrichment ratio reached 1.68. This result is consistent with the increased NO_3^- fraction in late-stage high-$PM_{2.5}$ samples in Sect. 3.1, indicating that the key source amplified during late-stage high-$PM_{2.5}$ conditions was secondary nitrate.

The main stage patterns and late-stage nitrate dominance were unchanged in the Fpeak = 0.5 sensitivity solution (Table S3b and Fig. S3).

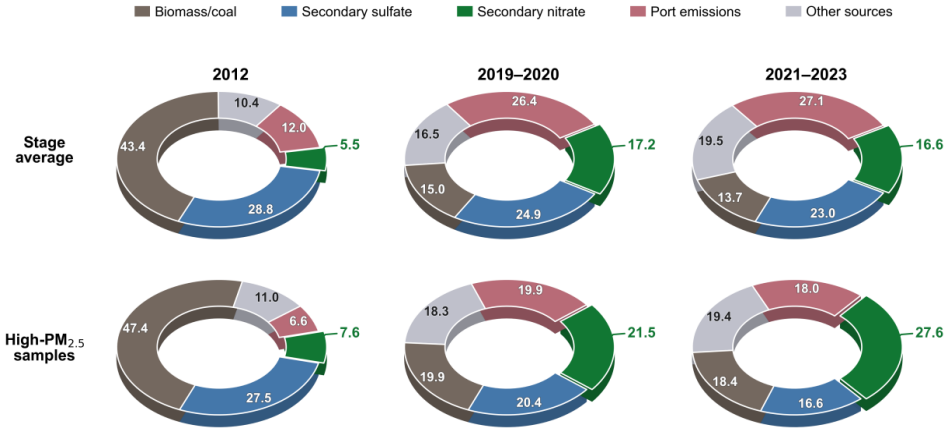

Figure 4. Comparison of PMF source contributions between stage-average samples and high-$PM_{2.5}$ samples. High-$PM_{2.5}$ samples were selected after mineral-dust outlier removal. Other sources comprise mineral dust, sea salt, and industrial metals.

3.3 Integrated discussion: high-$PM_{2.5}$ conditions, ion balance, and thermodynamic diagnostics

The chemical-composition and PMF results together indicate a stage-dependent reorganisation of $PM_{2.5}$ composition and source contributions. The decrease in EC is consistent with the decline in the biomass/coal combustion factor, while the decrease in SO_4^{2-} reflects weakened sulfate influence. In contrast, the increase in NO_3^- and the higher secondary nitrate contribution indicate a late-stage shift toward nitrate-related secondary processes, and this nitrate signal was further amplified in high-$PM_{2.5}$ samples. The following discussion examines how this transition may be related to emission controls and adjustment within the secondary inorganic aerosol system.

The weakening of primary combustion can be placed in the context of long-term emission controls. The 2013 Air Pollution Prevention and Control Action Plan focused on reducing emissions from coal combustion, boilers, and key industries, while the 2018 Three-Year Action Plan further promoted residential coal replacement, clean heating, ultra-low-emission retrofits, and diesel-truck controls (State Council of the People's Republic of China, 2013, 2018). In this study, EC decreased from 1.46 μg m^{-3} in 2012–2013 to 0.81 μg m^{-3} in 2021–2023, and the PMF biomass/coal combustion factor decreased from 43.37 % in 2012 to 13.74 % in 2021–2023. The profile and seasonality of F2 (biomass/coal combustion) are also consistent with heating-season coal combustion, biomass burning, and regional transport. National emission inventories show sustained decreases in SO_2, NO_x, CO, and primary particulate matter after clean-air actions, with early and strong reductions in coal-combustion

https://doi.org/10.5194/egusphere-2026-3299
Preprint. Discussion started: 6 August 2026

emissions and primary particulate matter emissions (Kong et al., 2024). Together, these observations support an emission-control context for the long-term weakening of primary-combustion signals.

Secondary inorganic components did not decrease in parallel with primary-combustion indicators. SO_4^{2-} decreased from 9.86 ± 8.33 to 4.10 ± 3.13 μg m^{-3}, whereas NO_3^- increased from 6.31 ± 6.42 to 8.51 ± 11.60 μg m^{-3}, and the NO_3^-/SO_4^{2-} ratio increased from 0.64 to 2.08. In PMF, secondary nitrate increased from 5.50 % to 16.59 %. This pattern indicates that emission reductions were accompanied by an internal shift in secondary inorganic aerosol, from sulfate influence toward stronger nitrate contribution. Previous studies have shown that SO_2 reductions after 2013 were generally larger than NO_x reductions, promoting a faster sulfate decrease. At the same time, declining SO_2 can reduce competition for NH_3/NH_4^+ from ammonium sulfate formation, allowing more NH_3/NH_4^+ to enter the ammonium nitrate equilibrium system (Liu et al., 2018; Meng et al., 2022; Zhai et al., 2021). Thus, even when NO_x emissions decline, nitrate can remain important under sufficient NH_3 supply, favourable humidity, and gas–particle partitioning conditions.

This nitrate amplification is particularly evident in late-stage high-$PM_{2.5}$ samples. In 2021–2023, NO_3^- accounted for 19.19 % of $PM_{2.5}$ in the highest 20 % $PM_{2.5}$ samples, compared with 12.44 % in the screened stage-average composition, whereas SO_4^{2-} decreased from 9.59 % to 5.97 % and OC+EC decreased from 7.19 % to 5.29 %. The PMF secondary nitrate contribution also increased from the stage-average value of 16.59 % to 27.59 % in high-$PM_{2.5}$ samples. These paired compositional and source-apportionment results indicate that late-stage high-$PM_{2.5}$ conditions were mainly associated with nitrate-related secondary formation and particle-phase accumulation.

To understand why nitrate accumulated more readily in the particle phase in the later stage, it is necessary to examine the partitioning of NH_4^+ between sulfate neutralisation and nitrate formation, together with aerosol liquid water and acid–base conditions. The ion-balance results provide this additional context (Fig. 5a, b). Because ALWC and some ion-balance indicators were skewed and a few high-humidity samples could disproportionately affect the mean, medians are used here to represent typical stage conditions. In 2012–2013, the median $NH_4^+/2SO_4^{2-}$ molar ratio was 0.61 and NH_4^+ excess was −0.047 μmol m^{-3}; in high-$PM_{2.5}$ samples, the corresponding values were 0.57 and −0.133 μmol m^{-3}. These values point to insufficient particulate NH_4^+ for complete SO_4^{2-} neutralisation in the early stage, so the sulfate system was closer to an incompletely neutralised state and conditions favouring particle-phase NO_3^- accumulation were weaker. In 2017–2020 and 2021–2023, the $NH_4^+/2SO_4^{2-}$ ratio increased to 2.09 and 1.66, respectively, and NH_4^+ excess became positive, at 0.053 and 0.044 μmol m^{-3}. In 2021–2023 high-$PM_{2.5}$ samples, the $NH_4^+/2SO_4^{2-}$ ratio further increased to 2.92 and NH_4^+ excess to 0.253 μmol m^{-3}. As SO_4^{2-} decreased, sulfate exerted a weaker neutralisation constraint on NH_4^+, leaving more particulate NH_4^+ available after sulfate neutralisation and thereby creating more favourable conditions for NH_4NO_3 formation.

The ISORROPIA-II metastable calculation provides a complementary thermodynamic diagnostic (Fig. 5c; Text S4, Table S6, and Fig. S7). Under the metastable state, the median aerosol liquid water content (ALWC) in 2021–2023 high-$PM_{2.5}$ samples was 22.00 μg m^{-3}, higher than 14.95 μg m^{-3} in 2012–2013 and 12.15 μg m^{-3} in 2017–2020. Median NO_3^- and NH_4^+ increased to 21.40 and 7.02 μg m^{-3}, respectively. NO_3^-, NH_4^+, and model-diagnosed aerosol liquid water content were all higher in late-stage high-$PM_{2.5}$ samples, collectively indicating more favourable conditions for NH_4NO_3 formation and persistence. Higher ALWC favours inorganic-salt hygroscopic growth and may promote HNO_3 and NH_3 partitioning to the particle phase, thereby supporting the formation and persistence of particle-phase NH_4NO_3. The pH diagnostic points to possible stage differences in aerosol acid–base conditions, but because synchronous gaseous NH_3, HNO_3, and HCl observations were unavailable, pH is used only as a model diagnostic to assess relative thermodynamic changes, not as independent mechanistic evidence (Fountoukis and Nenes, 2007; Song et al., 2018). The sensitivity of the diagnostic pH to ion charge balance is provided in Table S7 and Fig. S6.

https://doi.org/10.5194/egusphere-2026-3299
Preprint. Discussion started: 6 August 2026

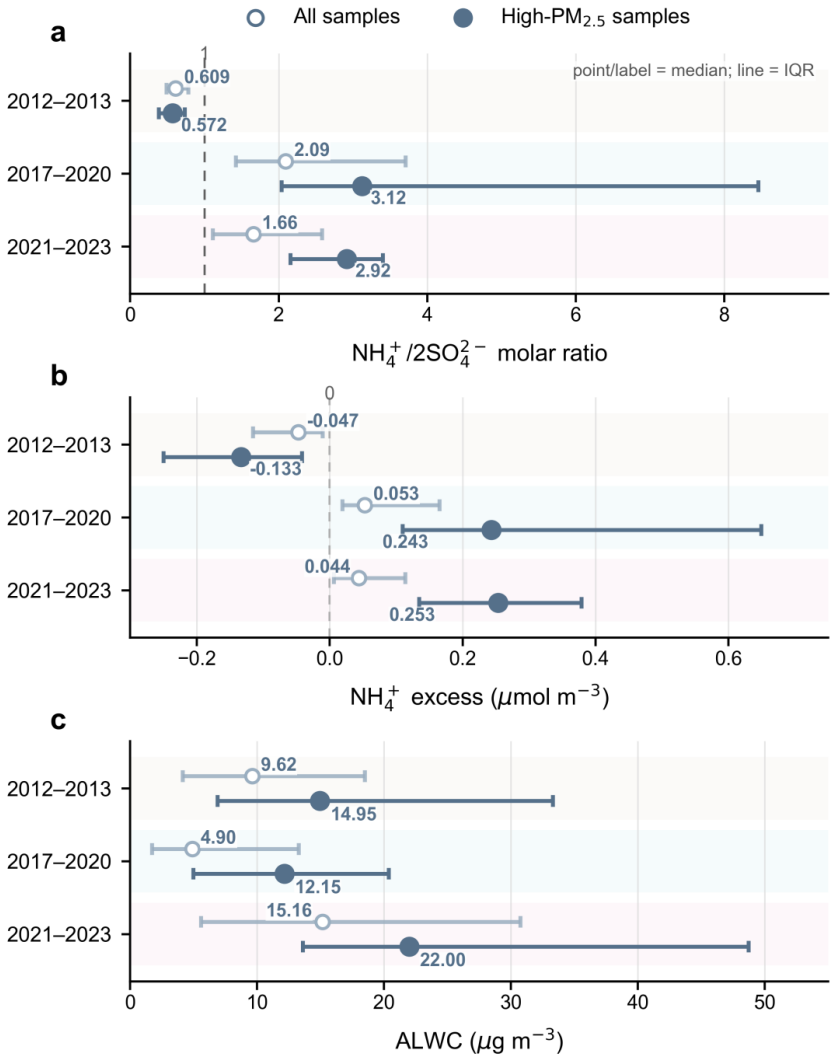

Figure 5. Stage changes in ion balance and aerosol liquid water content for all samples and high-$PM_{2.5}$ samples included in the ISORROPIA-II calculations. (a) $NH_4^+/2SO_4^{2-}$ molar ratio; (b) NH_4^+ excess after sulfate neutralisation; (c) aerosol liquid water content diagnosed under the ISORROPIA-II metastable state. Open points denote all samples and filled points denote high-$PM_{2.5}$ samples. Points and numbers show medians, and horizontal bars show the 25th–75th percentile range.

ISORROPIA-II stable-mode diagnostics of model-resolved solid salts show an increasing relative contribution of NH_4NO_3 within the modelled solid salts (Fig. S8). For all valid samples, NH_4NO_3 increased from 13.5 % in 2012–2013 to 48.3 % in 2021–2023. In high-$PM_{2.5}$ samples, the increase was stronger: NH_4NO_3 rose from 16.8 % to 59.2 % and became the largest model-resolved solid-salt component in 2017–2020 and 2021–2023. At the same time, $(NH_4)_2SO_4$ in high-$PM_{2.5}$ samples decreased from 26.8 % to 4.2 %, and the mean NH_4NO_3 concentration increased from 1.32 to 7.21 μg m^{-3}. As sulfate consumed less NH_4^+ for neutralisation, the model-resolved solid-salt composition in late-stage high-$PM_{2.5}$ samples shifted toward NH_4NO_3. Within this diagnostic framework, the shift toward NH_4NO_3, together with the increase in ALWC, supports the interpretation that late-stage nitrate amplification was more likely associated with NH_4NO_3 formation and particle-phase accumulation under wetter particle conditions.

https://doi.org/10.5194/egusphere-2026-3299
Preprint. Discussion started: 6 August 2026

This interpretation is consistent with previous evidence from North China, but the Tuoji Island record provides an independent long-term background perspective. Huang et al. (2014) and Guo et al. (2014) showed that rapid $PM_{2.5}$ accumulation during severe haze events is closely linked to secondary aerosol formation. Long-term source-apportionment studies in Tianjin also showed that, after clean-air actions, primary combustion or coal-related contributions declined, sulfate dominance weakened, and nitrate became more prominent in later-stage pollution (Dai et al., 2023). The added value of the Tuoji Island record is that it places evidence from earlier episode-based and urban studies within a long-term regional-background record spanning the emission-reduction trajectory from 2012 to 2023. It shows that combustion-signal weakening, sulfate decline, and nitrate enhancement are not limited to individual haze episodes or urban sites but also appear as a clear stage-dependent feature in a regional background record. From a control perspective, continued reduction of primary emissions remains necessary, but late-stage high-$PM_{2.5}$ pollution requires stronger coordinated control of NO_x, NH_3, and volatile organic compounds, together with attention to cold-season humid conditions and regional transport.

4 Conclusions

This study combined long-term $PM_{2.5}$ observations, chemical-composition data, and PMF source apportionment from Tuoji Island to examine stage-dependent changes in $PM_{2.5}$ composition and source structure, as well as the components amplified in high-$PM_{2.5}$ samples at a coastal background site in North China during 2012–2023. $PM_{2.5}$ mass did not decrease monotonically. Instead, the record indicates weakened primary-combustion signals, declining sulfate dominance, and late-stage amplification of secondary nitrate.

In terms of chemical composition, stage-mean $PM_{2.5}$ concentrations were 51.75 ± 36.99, 47.31 ± 35.52, and 54.41 ± 44.20 μg m^{-3} in 2012–2013, 2017–2020, and 2021–2023, respectively. Although stage-mean $PM_{2.5}$ did not decline monotonically, its major components changed substantially. EC decreased from 1.46 ± 0.94 to 0.81 ± 0.62 μg m^{-3}, and OC decreased from 3.83 ± 2.73 to 2.65 ± 2.05 μg m^{-3}, indicating a sustained weakening of carbonaceous primary-combustion signals across the observed stages. Over the same period, SO_4^{2-} decreased from 9.86 ± 8.33 to 4.10 ± 3.13 μg m^{-3}, whereas NO_3^- increased from 6.31 ± 6.42 to 8.51 ± 11.60 μg m^{-3}. The NO_3^-/SO_4^{2-} ratio therefore increased from 0.64 to 2.08 across the study periods, indicating a shift in the secondary inorganic aerosol system from sulfate dominance toward the greater relative importance of nitrate.

PMF results support the composition-based interpretation. In the comparable PMF sample set, which was constructed using the input species shared across the compared periods, the biomass/coal combustion contribution decreased from 43.37 % in 2012 to 13.74 % in 2021–2023, consistent with the EC decline. Over the same periods, the secondary nitrate contribution increased from 5.50 % to 16.59 %. These changes indicate a weakening combustion-related signal and an increasing role of secondary nitrate in the PMF-resolved mean source structure.

The high-$PM_{2.5}$ subset further shows that this nitrate-related source contribution was selectively amplified under polluted conditions. In 2021–2023, secondary nitrate reached 27.59 % in high-$PM_{2.5}$ samples, exceeding biomass/coal combustion (18.36 %), port emissions (18.02 %), and secondary sulfate (16.59 %); its enrichment ratio reached 1.68. Consistently, NO_3^- accounted for 19.19 % of $PM_{2.5}$ in 2021–2023 high-$PM_{2.5}$ samples, much higher than SO_4^{2-} at 5.97 % and OC+EC at 5.29 %. The NO_3^- enrichment factor was 1.54, whereas those for SO_4^{2-} and OC+EC were 0.62 and 0.73. The NO_3^-/SO_4^{2-} ratio in high-$PM_{2.5}$ samples increased from 0.76 in 2012–2013 to 3.42 in 2021–2023. At both the chemical-component and PMF source-apportionment levels, secondary nitrate was therefore the dominant amplified component and PMF-resolved source factor in late-stage high-$PM_{2.5}$ samples.

Ion-balance and ISORROPIA-II diagnostics further support this interpretation. In 2012–2013 high-$PM_{2.5}$ samples, the $NH_4^+/2SO_4^{2-}$ ratio was 0.57 and NH_4^+ excess was −0.133 μmol m^{-3}, indicating that particulate NH_4^+ was mainly constrained by sulfate neutralisation. By 2021–2023, the $NH_4^+/2SO_4^{2-}$ ratio increased to 2.92 and NH_4^+ excess increased to 0.253 μmol

https://doi.org/10.5194/egusphere-2026-3299
Preprint. Discussion started: 6 August 2026

m^{-3}, indicating greater NH_4^+ availability after sulfate neutralisation and more favourable conditions for NH_4NO_3 formation. In the same high-$PM_{2.5}$ samples, median ALWC increased to 22.00 μg m^{-3}, while median NO_3^- and NH_4^+ reached 21.40 and 7.02 μg m^{-3}, respectively, showing that nitrate, ammonium, and particle liquid water increased together in late-stage high-$PM_{2.5}$ samples.

Together, the composition, PMF, and thermodynamic diagnostics show that late-stage secondary nitrate amplification is not inferred from a single indicator. EC and biomass/coal combustion declined, so primary combustion did not explain the late-stage amplification observed in high-$PM_{2.5}$ samples. SO_4^{2-} and secondary sulfate weakened, while NO_3^-, secondary nitrate, NH_4^+ excess, model-diagnosed aerosol liquid water content, and NH_4NO_3-related solid-salt fractions increased. Late-stage high-$PM_{2.5}$ pollution at Tuoji Island was therefore more closely related to nitrate-related secondary processes under greater NH_4^+ availability and higher ALWC.

The Tuoji Island long-term record indicates that coastal-background $PM_{2.5}$ in North China has entered a stage in which sulfate-control benefits are evident but nitrate-control pressure is increasing. This trajectory is consistent with experience in the United States and Europe, where strong SO_2 controls produced large sulfate reductions, while nitrate and reduced-nitrogen chemistry remained harder to suppress (Hand et al., 2012; Hand et al., 2024; Tørseth et al., 2012). These experiences suggest that, after sulfate control becomes effective, $PM_{2.5}$ mitigation increasingly depends on coordinated management of nitrate, ammonium, and their precursors. Future control in North China should therefore consolidate reductions in coal combustion, industrial emissions, and primary particulate matter. It should also strengthen coordinated control of NO_x, NH_3, and VOCs, with particular attention to cold-season humid conditions and regional transport that favour particulate ammonium nitrate accumulation.

Code availability

No custom model code was developed in this study. EPA PMF 5.0 was used for source apportionment and is publicly available from the US Environmental Protection Agency. ISORROPIA-II was used for thermodynamic equilibrium calculations as described by Fountoukis and Nenes (2007).

Data availability

Summary data and robustness checks supporting the main figures are provided in the Supplement. Additional raw observational data are available from the corresponding author upon reasonable request because they form part of an ongoing long-term observation programme.

Supplement link

The supplementary material will be published as a separate file with this article.

Author contributions

Yuchen Li and Chongguo Tian conceptualised the study. Yuchen Li curated the data, performed the statistical analysis, PMF source apportionment, ISORROPIA-II calculations, and visualisation, and wrote the original draft. Zheng Zong contributed to PMF analysis and interpretation of source apportionment results. Xiaoping Wang, Xiaolan Shi, Zhineng Cheng, Ziyang Zhang, Zeyu Sun, Xuehua Yin, Zhifeng Lou, and Rong Sun contributed to sample collection, chemical measurements, and data quality control. Roland Kallenborn provided scientific consultation and contributed to manuscript review, editing, and English-language polishing. All authors contributed to the discussion of the results and reviewed and edited the manuscript.

https://doi.org/10.5194/egusphere-2026-3299
Preprint. Discussion started: 6 August 2026

Competing interests

The authors declare that they have no conflict of interest.

Disclaimer

Copernicus Publications remains neutral with regard to jurisdictional claims in published maps and institutional affiliations.

Acknowledgements

The authors thank the staff of the Tuoji Island observation site for their assistance with sample collection and field maintenance. The authors also thank the laboratory and technical staff involved in chemical analysis and data quality control.

Financial support

This research has been supported by the Open Research Fund of Key Laboratory of Land and Sea Ecological Governance and Systematic Regulation (grant no. LSEGSR202402), and the National Natural Science Foundation of China (grant no. 42177089).

References

Brown, S. G., Eberly, S., Paatero, P., and Norris, G. A.: Methods for estimating uncertainty in PMF solutions: examples with ambient air and water quality data and guidance on reporting PMF results, Sci. Total Environ., 518–519, 626–635, https://doi.org/10.1016/j.scitotenv.2015.01.022, 2015.

Cao, J. J., Wu, F., Chow, J. C., Lee, S. C., Li, Y., Chen, S. W., An, Z. S., Fung, K. K., Watson, J. G., Zhu, C. S., and Liu, S. X.: Characterization and source apportionment of atmospheric organic and elemental carbon during fall and winter of 2003 in Xi'an, China, Atmos. Chem. Phys., 5, 3127–3137, https://doi.org/10.5194/acp-5-3127-2005, 2005.

Cao, J., Zheng, B., Chen, J., and Liu, Y.: Assessment of sulfate and nitrate variations in China during 1990–2020: Insights into source contributions and formation pathways, J. Hazard. Mater., 489, 137600, https://doi.org/10.1016/j.jhazmat.2025.137600, 2025.

Chang, C. C., Yuan, C. S., Li, T. C., Su, Y. L., Tong, C., and Wu, S. P.: Chemical characteristics, source apportionment, and regional transport of marine fine particles toward offshore islands near the coastline of northwestern Taiwan Strait, Environ. Sci. Pollut. Res., 25, 32332–32345, https://doi.org/10.1007/s11356-018-3093-9, 2018.

Chow, J. C., Watson, J. G., Chen, L. W. A., Chang, M. C. O., Robinson, N. F., Trimble, D., and Kohl, S.: The IMPROVE_A Temperature Protocol for Thermal/Optical Carbon Analysis: Maintaining Consistency with a Long-Term Database, J. Air Waste Manag. Assoc., 57, 1014–1023, https://doi.org/10.3155/1047-3289.57.9.1014, 2007.

Dai, Q., Chen, J., Wang, X., Dai, T., Tian, Y., Bi, X., Shi, G., Wu, J., Liu, B., Zhang, Y., Yan, B., Kinney, P. L., Feng, Y., and Hopke, P. K.: Trends of source apportioned $PM_{2.5}$ in Tianjin over 2013–2019: Impacts of Clean Air Actions, Environ. Pollut., 325, 121344, https://doi.org/10.1016/j.envpol.2023.121344, 2023.

DeBell, L. J., Vozzella, M., Talbot, R. W., and Dibb, J. E.: Asian dust storm events of spring 2001 and associated pollutants observed in New England by the Atmospheric Investigation, Regional Modeling, Analysis and Prediction (AIRMAP) monitoring network, J. Geophys. Res., 109, D01304, https://doi.org/10.1029/2003JD003733, 2004.

Feng, T., Li, G., Zhao, S., Bei, N., Long, X., Pan, Y., Song, Y., Wang, R., Tie, X., and Molina, L. T.: Fertilization-driven pulses of atmospheric nitrogen dioxide complicate air pollution in early spring over the North China Plain, Atmos. Chem. Phys., 25, 11703–11718, https://doi.org/10.5194/acp-25-11703-2025, 2025.

https://doi.org/10.5194/egusphere-2026-3299
Preprint. Discussion started: 6 August 2026

Fountoukis, C., and Nenes, A.: ISORROPIA II: a computationally efficient thermodynamic equilibrium model for K^+–Ca^{2+}–Mg^{2+}–NH_4^+–Na^+–SO_4^{2-}–NO_3^-–Cl^-–H_2O aerosols, Atmos. Chem. Phys., 7, 4639–4659, https://doi.org/10.5194/acp-7-4639-2007, 2007.

Gao, M., Carmichael, G. R., Saide, P. E., Lu, Z., Yu, M., Streets, D. G., and Wang, Z.: Response of winter fine particulate matter concentrations to emission and meteorology changes in North China, Atmos. Chem. Phys., 16, 11837–11851, https://doi.org/10.5194/acp-16-11837-2016, 2016.

Guo, S., Hu, M., Zamora, M. L., Peng, J., Shang, D., Zheng, J., Du, Z., Wu, Z., Shao, M., Zeng, L., Molina, M. J., and Zhang, R.: Elucidating severe urban haze formation in China, Proc. Natl. Acad. Sci. U.S.A., 111, 17373–17378, https://doi.org/10.1073/pnas.1419604111, 2014.

Hand, J. L., Schichtel, B. A., Malm, W. C., and Pitchford, M. L.: Particulate sulfate ion concentration and SO_2 emission trends in the United States from the early 1990s through 2010, Atmos. Chem. Phys., 12, 10353–10365, https://doi.org/10.5194/acp-12-10353-2012, 2012.

Hand, J. L., Prenni, A. J., and Schichtel, B. A.: Trends in seasonal mean speciated aerosol composition in remote areas of the United States from 2000 through 2021, J. Geophys. Res.-Atmos., 129, e2023JD039902, https://doi.org/10.1029/2023JD039902, 2024.

Huang, R. J., Zhang, Y., Bozzetti, C., Ho, K. F., Cao, J. J., Han, Y., Daellenbach, K. R., Slowik, J. G., Platt, S. M., Canonaco, F., Zotter, P., Wolf, R., Pieber, S. M., Bruns, E. A., Crippa, M., Ciarelli, G., Piazzalunga, A., Schwikowski, M., Abbaszade, G., Schnelle-Kreis, J., Zimmermann, R., An, Z., Szidat, S., Baltensperger, U., Haddad, I. E., and Prévôt, A. S. H.: High secondary aerosol contribution to particulate pollution during haze events in China, Nature, 514, 218–222, https://doi.org/10.1038/nature13774, 2014.

Kong, L., Tang, X., Wang, Z., Zhu, J., Li, J., Wu, H., Wu, Q., Chen, H., Zhu, L., Wang, W., Liu, B., Wang, Q., Chen, D., Pan, Y., Li, J., Wu, L., and Carmichael, G. R.: Changes in air pollutant emissions in China during two clean-air action periods derived from the newly developed Inversed Emission Inventory for Chinese Air Quality (CAQIEI), Earth Syst. Sci. Data, 16, 4351–4387, https://doi.org/10.5194/essd-16-4351-2024, 2024.

Li, M., Hu, M., Guo, Q., Tan, T., Du, B., Huang, X., He, L., Guo, S., Wang, W., Fan, Y., and Xu, D.: Seasonal Source Apportionment of $PM_{2.5}$ in Ningbo, a Coastal City in Southeast China, Aerosol Air Qual. Res., 18, 2741–2752, https://doi.org/10.4209/aaqr.2018.01.0011, 2018.

Liu, B., Wang, Y., Meng, H., Dai, Q., Diao, L., Wu, J., Shi, L., Wang, J., Zhang, Y., and Feng, Y.: Dramatic changes in atmospheric pollution source contributions for a coastal megacity in northern China from 2011 to 2020, Atmos. Chem. Phys., 22, 8597–8615, https://doi.org/10.5194/acp-22-8597-2022, 2022.

Liu, M., Huang, X., Song, Y., Xu, T., Wang, S., Wu, Z., Hu, M., Zhang, L., Zhang, Q., Pan, Y., Liu, X., and Zhu, T.: Rapid SO_2 emission reductions significantly increase tropospheric ammonia concentrations over the North China Plain, Atmos. Chem. Phys., 18, 17933–17943, https://doi.org/10.5194/acp-18-17933-2018, 2018.

Liu, T., Hu, B., Yang, Y., Li, M., Hong, Y., Xu, X., Xu, L., Chen, N., Chen, Y., Xiao, H., and Chen, J.: Characteristics and source apportionment of $PM_{2.5}$ on an island in Southeast China: Impact of sea-salt and monsoon, Atmos. Res., 235, 104786, https://doi.org/10.1016/j.atmosres.2019.104786, 2020.

Liu, Z., Qi, J., Ni, Y., Xue, L., and Liu, X.: Enhanced atmospheric oxidation and particle reductions driving changes to nitrate formation mechanisms across coastal and inland regions of north China, Atmos. Chem. Phys., 25, 8719–8742, https://doi.org/10.5194/acp-25-8719-2025, 2025.

MEE (Ministry of Ecology and Environment of the People's Republic of China): Technical specifications on ambient air quality index (HJ 633–2026), Ministry of Ecology and Environment of the People's Republic of China, https://www.mee.gov.cn/ywgz/fgbz/bz/bzwb/jcffbz/202602/t20260225_1144441.shtml, 2026.

https://doi.org/10.5194/egusphere-2026-3299
Preprint. Discussion started: 6 August 2026

Meng, F., Zhang, Y., Kang, J., Heal, M. R., Reis, S., Wang, M., Liu, L., Wang, K., Yu, S., Li, P., Wei, J., Hou, Y., Zhang, Y., Liu, X., Cui, Z., Xu, W., and Zhang, F.: Trends in secondary inorganic aerosol pollution in China and its responses to emission controls of precursors in wintertime, Atmos. Chem. Phys., 22, 6291–6308, https://doi.org/10.5194/acp-22-6291-2022, 2022.

MEP (Ministry of Environmental Protection of the People's Republic of China): Ambient air quality standards (GB 3095–2012), China Environmental Science Press, Beijing, China, 2012.

Norris, G., Duvall, R., Brown, S., and Bai, S.: EPA Positive Matrix Factorization (PMF) 5.0 Fundamentals and User Guide. U.S. Environmental Protection Agency, EPA/600/R-14/108, 2014.

Paatero, P., and Tapper, U.: Positive matrix factorization: A non-negative factor model with optimal utilization of error estimates of data values, Environmetrics, 5, 111–126, https://doi.org/10.1002/env.3170050203, 1994.

Paatero, P.: Least squares formulation of robust non-negative factor analysis, Chemometr. Intell. Lab., 37, 23-35, https://doi.org/10.1016/S0169-7439(96)00044-5, 1997.

Pathak, R. K., Wu, W. S., and Wang, T.: Summertime $PM_{2.5}$ ionic species in four major cities of China: nitrate formation in an ammonia-deficient atmosphere, Atmos. Chem. Phys., 9, 1711–1722, https://doi.org/10.5194/acp-9-1711-2009, 2009.

Pui, D. Y. H., Chen, S. C., and Zuo, Z.: $PM_{2.5}$ in China: Measurements, sources, visibility and health effects, and mitigation, Particuology, 13, 1-26, https://doi.org/10.1016/j.partic.2013.11.001, 2014.

Song, S., Gao, M., Xu, W., Shao, J., Shi, G., Wang, S., Wang, Y., Sun, Y., and McElroy, M. B.: Fine-particle pH for Beijing winter haze as inferred from different thermodynamic equilibrium models, Atmos. Chem. Phys., 18, 7423–7438, https://doi.org/10.5194/acp-18-7423-2018, 2018.

State Council of the People's Republic of China: Notice of the State Council on issuing the Air Pollution Prevention and Control Action Plan (Guo Fa [2013] No. 37), Ministry of Ecology and Environment of the People's Republic of China, https://www.mee.gov.cn/ywgz/zcghtjdd/sthjghjh/201811/t20181129_676555.shtml, 2013.

State Council of the People's Republic of China: Notice of the State Council on issuing the Three-Year Action Plan for Winning the Blue Sky Defence Battle (Guo Fa [2018] No. 22), Ministry of Ecology and Environment of the People's Republic of China, https://www.mee.gov.cn/zcwj/gwywj/201807/t20180704_446068.shtml, 2018.

Su, X., Wang, Q., Li, Z., Calvello, M., Esposito, F., Pavese, G., Lin, M., Cao, J., Zhou, C., Li, D., and Xu, H.: Regional transport of anthropogenic pollution and dust aerosols in spring to Tianjin — A coastal megacity in China, Sci. Total Environ., 584–585, 381–392, https://doi.org/10.1016/j.scitotenv.2017.01.016, 2017.

Tang, M., Liu, Y., He, J., Wang, Z., Wu, Z., and Ji, D.: In situ continuous hourly observations of wintertime nitrate, sulfate and ammonium in a megacity in the North China plain from 2014 to 2019: Temporal variation, chemical formation and regional transport, Chemosphere, 262, 127745, https://doi.org/10.1016/j.chemosphere.2020.127745, 2021.

Tørseth, K., Aas, W., Breivik, K., Fjæraa, A. M., Fiebig, M., Hjellbrekke, A. G., Lund Myhre, C., Solberg, S., and Yttri, K. E.: Introduction to the European Monitoring and Evaluation Programme (EMEP) and observed atmospheric composition change during 1972–2009, Atmos. Chem. Phys., 12, 5447–5481, https://doi.org/10.5194/acp-12-5447-2012, 2012.

Wang, X., Bi, X., Sheng, G., and Fu, J.: Chemical composition and sources of PM_{10} and $PM_{2.5}$ aerosols in Guangzhou, China, Environ. Monit. Assess., 119, 425–439, https://doi.org/10.1007/s10661-005-9034-3, 2006.

Wang, J., Gao, J., Che, F., Wang, Y., Lin, P., and Zhang, Y.: Decade-long trends in chemical component properties of $PM_{2.5}$ in Beijing, China (2011−2020), Sci. Total Environ., 832, 154664, https://doi.org/10.1016/j.scitotenv.2022.154664, 2022.

Wu, S. P., Schwab, J., Yang, B. Y., Zheng, A., and Yuan, C. S.: Two-Years $PM_{2.5}$ Observations at Four Urban Sites along the Coast of Southeastern China, Aerosol Air Qual. Res., 15, 1799–1812, https://doi.org/10.4209/aaqr.2015.05.0363, 2015.

Wu, X., Kong, Q., Lan, Y., Sng, J., and Yu, L. E.: Refined Sea Salt Markers for Coastal Cities Facilitating Quantification of Aerosol Aging and $PM_{2.5}$ Apportionment, Environ. Sci. Technol., 58, 8432–8443, https://doi.org/10.1021/acs.est.3c10142, 2024.

https://doi.org/10.5194/egusphere-2026-3299
Preprint. Discussion started: 6 August 2026

Xiao, H. W., Chen, T. S., Guan, C. F., Yin, M. J., Xiao, H., Xu, Y., and Xiao, H. Y.: Trans-regional NO_2 drives winter nitrate source and formation disparities between the North China Plain and the Yangtze River Delta, J. Hazard. Mater., 499, 140241, https://doi.org/10.1016/j.jhazmat.2025.140241, 2025.

Yang, T., Tian, Y., and Wang, Z.: Unveiling the critical role of tall-stack emissions in winter nitrate episodes over North China through machine learning and 3D model analysis, Front. Environ. Sci., 13, 1718020, https://doi.org/10.3389/fenvs.2025.1718020, 2025.

Yen, P. H., Yuan, C. S., Soong, K. Y., Jeng, M. S., and Cheng, W. H.: Identification of potential source regions and long-range transport routes/channels of marine $PM_{2.5}$ at remote sites in East Asia, Sci. Total Environ., 915, 170110, https://doi.org/10.1016/j.scitotenv.2024.170110, 2024.

Zhai, S., Jacob, D. J., Wang, X., Liu, Z., Wen, T., Shah, V., Li, K., Moch, J. M., Bates, K. H., Song, S., Shen, L., Zhang, Y., Luo, G., Yu, F., Sun, Y., Wang, L., Qi, M., Tao, J., Gui, K., Xu, H., Zhang, Q., Zhao, T., Wang, Y., Lee, H. C., Choi, H., and Liao, H.: Control of particulate nitrate air pollution in China, Nat. Geosci., 14, 389–395, https://doi.org/10.1038/s41561-021-00726-z, 2021.

Zhang, Y., Yang, L., Bie, S., Zhao, T., Huang, Q., Li, J., Wang, P., Wang, Y., and Wang, W.: Chemical compositions and the impact of sea salt in atmospheric PM_1 and $PM_{2.5}$ in the coastal area, Atmos. Res., 250, 105323, https://doi.org/10.1016/j.atmosres.2020.105323, 2021.

Zong, Z., Wang, X., Tian, C., Chen, Y., Qu, L., Ji, L., Zhi, G., Li, J., and Zhang, G.: Source apportionment of $PM_{2.5}$ at a regional background site in North China using PMF linked with radiocarbon analysis: insight into the contribution of biomass burning, Atmos. Chem. Phys., 16, 11249–11265, https://doi.org/10.5194/acp-16-11249-2016, 2016.